Paleoceanography and Paleoclimatology

RESEARCH ARTICLE
10.1029/2020PA003973

Influence of Elevated Nd Fluxes on the Northern Nd Isotope End Member of the Atlantic During the Early Holocene

Frerk Pöppelmeier[1,2], Jeemijn Scheen[1], Patrick Blaser[2], Jörg Lippold[2], Marcus Gutjahr[3], and Thomas F. Stocker[1]

[1]Climate and Environmental Physics, Physics Institute and Oeschger Centre for Climate Change Research, University of Bern, Bern, Switzerland, [2]Institute of Earth Sciences, Heidelberg University, Heidelberg, Germany, [3]GEOMAR Helmholtz Center for Ocean Research Kiel, Kiel, Germany

Key Points:
- Improved implementation of Nd sources and sinks in the Bern3D model provides better agreement with observational data
- Elevated Nd fluxes into the northern Northwest Atlantic caused northern end member shift as observed during the early Holocene
- Variations in the strength of the Atlantic meridional overturning produce different Nd isotope distributions than end member shifts

Supporting Information:
- Supporting Information S1
- Table S1

Correspondence to:
F. Pöppelmeier,
frerk.poeppelmeier@climate.unibe.ch

Citation:
Pöppelmeier, F., Scheen, J., Blaser, P., Lippold, J., Gutjahr, M., & Stocker, T. F. (2020). Influence of elevated Nd fluxes on the northern Nd isotope end member of the Atlantic during the early Holocene. *Paleoceanography and Paleoclimatology*, *35*, e2020PA003973. https://doi.org/10.1029/2020PA003973

Received 7 MAY 2020
Accepted 22 OCT 2020
Accepted article online 29 OCT 2020

Abstract The neodymium (Nd) isotopic composition of seawater is a valuable tool for the reconstruction of past water mass provenance and hence deep water geometry. A meaningful interpretation of Nd isotope down-core records requires knowledge of potential variations of water mass end member characteristics. While often assumed temporally constant, recent investigations revealed glacial-interglacial variability of the northern and southern Nd isotope end members in the Atlantic. These new constraints have a strong influence on the interpretation of the Atlantic deep water mass evolution, yet the processes responsible for the end member shifts remain uncertain. Here we combine a new compilation of Atlantic Nd isotope reconstructions of the early Holocene with the Nd-enabled Bern3D model to quantify the recently proposed hypothesis of a northern Nd isotope end member shift during the early Holocene. We achieve the best model-data fit with a strong increase of the Nd flux in the northern high latitudes by a factor of 3 to 4, which lowers the northern end member signature by about 1 ε-unit. Our findings thus agree with the rationale that glacially weathered material entered the northern Northwest Atlantic after the ice sheets retreated late in the deglaciation and released substantial amounts of unradiogenic Nd as suggested previously. Further, we find that variations in the strength of the Atlantic Meridional Overturning Circulation (AMOC) cannot reproduce the observed Nd isotope excursions of the compiled data, ruling out an early Holocene AMOC "overshoot."

1. Introduction

Over the past decade, the neodymium (Nd) isotopic composition—denoted as ε_{Nd}, which is the deviation of $^{143}Nd/^{144}Nd$ from the *Chondritic Uniform Reservoir* (Jacobsen & Wasserburg, 1980) in parts per ten thousand—of seawater has been widely applied as a tracer for past water mass provenance (e.g., Howe et al., 2017; Piotrowski et al., 2005; van de Flierdt et al., 2010). Independent of biological processes, the Nd isotopic composition provides an opportunity to disentangle changes in water mass structure from variations in the rate of remineralization of respired carbon. Modern observations confirm the quasi-conservative behavior of ε_{Nd} (van de Flierdt et al., 2016), but nonconservative processes may also play a role on local to regional scales (Haley et al., 2017; Rahlf et al., 2020). Today, three main water masses dominate the Atlantic Ocean, which are also distinguishable by their Nd isotopic composition. North Atlantic Deep Water (NADW), formed in the marginal seas of the North Atlantic, exhibits an ε_{Nd} value of around −13 (Lambelet et al., 2016) and is sandwiched between two southern sourced water masses: at intermediate-depth Antarctic Intermediate Water (AAIW) and at abyssal depth Antarctic Bottom Water (AABW), both exhibiting values between −8 and −9 (Stichel et al., 2012). For paleoceanographic investigations, knowledge about these end member constraints is imperative to faithfully reconstruct past water mass mixing. Recent studies showed that both northern and southern end members have varied considerably since the Last Glacial Maximum (LGM) (Huang et al., 2020; Pöppelmeier et al., 2019; Zhao et al., 2019). However, the origins of these end member changes remain speculative up to now (Howe et al., 2016; Huang et al., 2020; Pöppelmeier et al., 2019; Roberts & Piotrowski, 2015).

In order to improve the understanding of the Nd isotope response to AMOC variations, ε_{Nd} has been simulated in a handful of models (Arsouze et al., 2007, 2009; Friedrich et al., 2014; Gu et al., 2019;

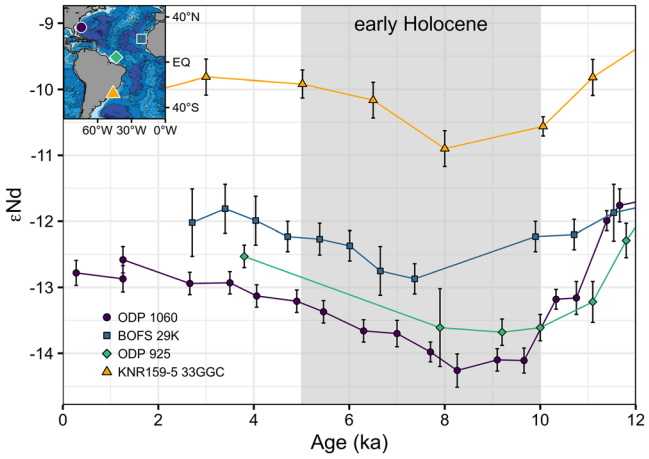

Figure 1. Selection of representative Holocene ε_{Nd} records exhibiting the early Holocene anomaly. Locations of the different sites are depicted on the map inset (ODP 1060, Pöppelmeier et al., 2019; BOFS 29K and ODP 925, Howe et al., 2017; KNR159-5 33GGC, Pöppelmeier et al., 2020). Temporal differences of the early Holocene ε_{Nd} minimum between sites can be assumed to be due to uncertainties in the age models.

Rempfer et al., 2011; Siddall et al., 2008). Two different approaches were used in these studies. First, a simplified implementation of ε_{Nd} as a passive tracer that only changes at the continental margins (Arsouze et al., 2007; Friedrich et al., 2014) and, second, a comprehensive implementation of the Nd cycle with all its known sources and sinks (Arsouze et al., 2009; Gu et al., 2019; Rempfer et al., 2011; Siddall et al., 2008). All these studies confirmed the quasi-conservative behavior of ε_{Nd} on interbasin scale and thus its sensitivity to changes in water mass provenance.

Recently, Howe et al. (2016) and Pöppelmeier et al. (2019) introduced the idea of an end member shift for the northern ε_{Nd} end member during the early Holocene to explain lower than modern ε_{Nd} values observed throughout the Atlantic during that time (Figure 1; e.g., Howe et al., 2017; Lippold et al., 2016; Pöppelmeier et al., 2018). The authors proposed that the end member shift was induced by changes of the Nd fluxes into the Labrador Sea due to input of poorly weathered material, originating from Greenland and North America, after the ice sheets retreated. This hypothesis presents a unique opportunity to test the influence of changing Nd fluxes on ε_{Nd} end member signatures, since the climatic and oceanic boundary conditions are thought to have been relatively stable throughout the entire Holocene (Andersen et al., 2004; Lippold et al., 2019). As such, variations in Atlantic ε_{Nd} reconstructions were most likely controlled by changes in the end member compositions and not in water mass mixing.

Here, we compile published and new authigenic Nd isotope reconstructions of the Atlantic to calculate early to late Holocene ε_{Nd} deviations (see Table S1 in the supporting information). Thus, we obtain a spatial distribution of the early Holocene ε_{Nd} anomaly, which allows us to identify the origin of the end member change. To further test our hypothesis, we employ the Nd-enabled Bern3D model (Rempfer et al., 2011), which we improved and extended to better represent recent findings regarding the sources and sinks of Nd (e.g., Haley et al., 2017; Rousseau et al., 2015). By varying the Nd supply to the Labrador Sea, the proposed source region, we can test the hypothesis and quantify the elevated Nd flux as well as its impact on the global distribution of Nd isotope signatures.

2. Materials and Methods

To quantitatively assess the influence of elevated Nd fluxes due to increased weathering on the northern ε_{Nd} end member, we compare Holocene Atlantic ε_{Nd} reconstructions compiled here to sensitivity tests performed with the Bern3D model.

2.1. Bern3D Model

The Bern3D model is an isotope enabled Earth System Model of Intermediate Complexity (Müller et al., 2006) coupled to a single-layer energy-moisture balance model (Ritz et al., 2011). The spatial resolution is 41 × 40 grid cells with 32 logarithmically scaled depth layers in the ocean. A detailed description of the physical and biogeochemical model components is given in the supporting information.

Nd isotopes were previously implemented by Rempfer et al. (2011) in an older version of the Bern3D model. Here we adapted the Nd-module for the new version v2.0, which exhibits a higher spatial resolution (Figure 2), and further improved the Nd-module of the Bern3D model as follows. In Rempfer et al. (2011) three sources (dust, rivers, and continental margins; Figures 3a–3c) and one sink (reversible scavenging) were implemented. The main Nd source to the oceans was the boundary source, contributing ~90% to the total budget. This was implemented as a constant Nd flux from all vertical sediment-water interfaces shallower than 3,000 m. In recent years, several studies showed that this simplification may need to be revised (e.g., Abbott, 2019; Abbott et al., 2015). Instead, observations indicate that an Nd flux into bottom waters occurs at all sediment-water interfaces, independent of the water depth (Haley et al., 2017). Deposition of reactive material (e.g., volcanic ash) and nepheloid layers might further amplify this benthic Nd flux on local to regional scale (Blaser et al., 2020; Elmore et al., 2011; Pöppelmeier et al., 2019). As such, we removed the

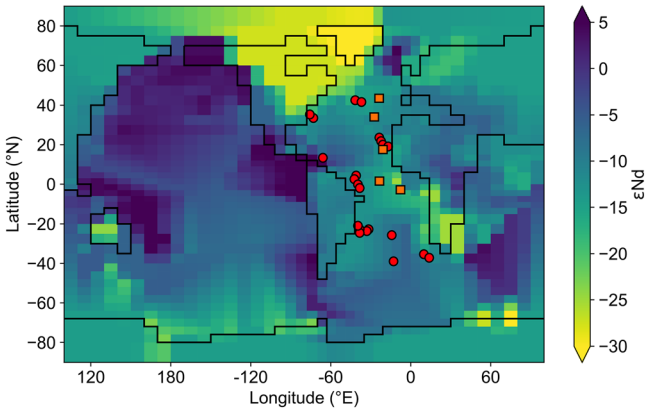

Figure 2. Global map of the Nd isotopic compositions of the benthic flux used in the Bern3D model linearly extrapolated from the database by Jeandel et al. (2007) with further constraints from Blanchet (2019). Locations of published and new Holocene εNd records are depicted as red circles and orange squares, respectively. See Table S1 for core locations and references.

depth limitation of the benthic Nd flux in the Bern3D model with Nd now escaping all vertical as well as horizontal sediment-water interfaces, which leads to a redistribution of this Nd source from the margins to the open ocean compared to Rempfer et al. (2011). Further, we added a scaling factor for the benthic Nd flux in each grid cell adjacent to the sediment (α_{bs}) in order to better represent local features through increased benthic sources (Figure 3d), as observed in the modern ocean (see the supporting information text and Figures S1 to S3 for details; e.g., Abbott et al., 2015; Blaser et al., 2020; Grenier et al., 2013; Lacan & Jeandel, 2005; Rahlf et al., 2020). The scaling factor is assumed to vary only on large spatial scales and takes discrete values of 1, 2, or 3 (see Figure 3d). It was regionally extrapolated based on modern observations. In a second approach for the estimation of α_{bs}, we assumed that the benthic flux influences the pore water, and hence authigenic phases, more strongly than the bottom water. This would lead to core top-bottom water offsets, which we then assumed to be a measure for the strength of the benthic Nd flux (see the supporting information and Figures S1 to S3 for details). This approach is in relatively good agreement with our first approach, except for the Cape Basin and the North Pacific. Responsible for the latter is the lack of core-top data, while seawater data found evidence for benthic Nd addition in the Cape Basin without discernible changes in the Nd isotopic composition. This effect is presumably due to the similarity of detrital and bottom water ε_{Nd} (Rahlf et al., 2020). The Nd isotope signatures of the benthic flux are based on a global linear extrapolation of the database of detrital sediment and continental signatures by Jeandel et al. (2007) with further constraints from the database by Blanchet (2019) (Figure 2).

Further, we updated the parameters for the riverine Nd source (water discharge, Nd concentration, and ε_{Nd}) that were based on the compilation by Goldstein and Jacobsen (1987) with other observations

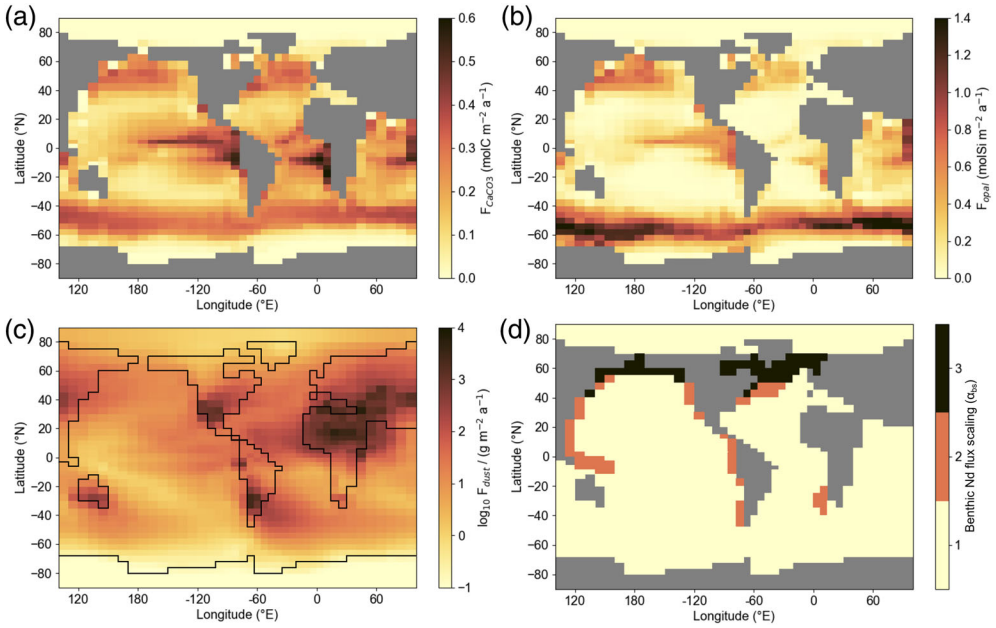

Figure 3. (a) Global export production of $CaCO_3$ in mol C/(m^2 a) and (b) biogenic opal flux in mol Si/(m^2 a) calculated from nutrient concentrations, temperature, and light. (c) Log10 of annual mean dust deposition for the preindustrial after Mahowald et al. (2006). See Figure S6 for ε_{Nd} of the dust source. (d) Map of benthic Nd flux scaling (α_{bs}) used in the control run, which is estimated from observations of elevated fluxes (Abbott et al., 2015; Blaser et al., 2020; Lacan & Jeandel, 2005). Only the cells in the North Atlantic with $\alpha_{bs} > 1$ were modified in the sensitivity tests described in section 3.1. In these test, the values of α_{bs} were multiplied by 2, 3, 4, or 5. An alternative choice for α_{bs} is shown in Figure S2.

(Casse et al., 2019; Dai & Trenberth, 2002; Goldstein & Jacobsen, 1988; Rahlf et al., 2020; Rousseau et al., 2015). Finally, we introduced a new scaling factor for the riverine source α_{ri} as a tuning parameter, based on recent findings by Rousseau et al. (2015), showing that resuspended riverine sediments partly dissolve in the estuary and hence release Nd in substantial amounts. These authors investigated this phenomenon at the Amazon River, where up to four times more Nd was released by the estuary sediments than was supplied in dissolved form by the river. A global extrapolation of their findings suggests that this Nd source could be up to 6–17 times larger than the dissolved riverine Nd source (Rousseau et al., 2015).

The model distribution of desert dust was updated based on Mahowald et al. (2006) (Figure 3c), but the Nd concentration of 20 ppm and dissolution of 2% were unchanged from Rempfer et al. (2011). As a consequence, Nd from dust dissolution nearly doubled since the implementation by Rempfer et al. (2011) from 0.26×10^9 g/a to 0.50×10^9 g/a here. Details on the differences between the first implementation by Rempfer et al. (2011) and the update here are summarized in Table S2.

Because the Nd sources and their distributions changed substantially in the model since the implementation by Rempfer et al. (2011), we retuned the Nd module by minimizing the mean absolute error (MAE) of the dissolved Nd concentration and ε_{Nd} (weighted by the provided measurement uncertainty) between the Bern3D model and the updated NEOSYMPA database of observational data (Tachikawa et al., 2017). In this updated version we included the most recent studies (Amakawa et al., 2019; Rahlf et al., 2020; Stichel et al., 2018; Zieringer et al., 2019). Note that seawater data are biased toward the Atlantic (~50% of all data) as well as toward shallower water depths (median water depth = 600 m). Since ε_{Nd} and the dissolved Nd concentration do not always agree between filtered and unfiltered seawater samples, hinting toward particle dissolution during sample processing, we excluded all unfiltered data from the database. For the tuning of the Nd module we further did not consider observational data from water depths shallower than 250 m. The rationale for this is that surface water Nd characteristics are often dominated by local features such as volcanic islands that have disproportional influence on surface water ε_{Nd} due to low Nd concentrations (e.g., Stichel et al., 2015; Zieringer et al., 2019). As a result of the low spatial resolution, such features are not represented in the Bern3D model. Tuning parameters for the Nd-module are the total benthic Nd flux, the scavenging efficiency, and the scaling factor for the riverine source associated with the findings by Rousseau et al. (2015). All simulations were run under preindustrial boundary conditions for 5,000 years, which was sufficient to achieve steady state.

2.2. Sediment Cores

We compiled authigenic Nd isotope reconstructions from the Atlantic (45°S to 45°N) that are considered not to be overprinted by in situ effects (i.e., core tops in agreement of ±1 ε-unit with proximate seawater data) and hence represent the local bottom water Nd isotope signature while covering the time period of the early to mid-Holocene. We consider all archives (foraminifera, fish debris, and leaches) as long as the authors provided evidence that the extracted signal is of authigenic origin. In addition, we present new ε_{Nd} records from five sites located in the deep Atlantic. Detailed information on location, water depth, and age control can be found in Tables S1 and S5. To estimate the early Holocene anomaly in ε_{Nd} from the modern, the minimum value in the time range from 5 to 10 ka Before Present (BP) was subtracted from the average in the time interval of 0–2 ka BP. For sites without data covering the late Holocene, the modern seawater value from the nearest station was taken.

For the new sites the authigenic Nd fraction was extracted from the bulk sediment following the gentle leaching protocol by Blaser et al. (2016). This has proven to reliably extract the authigenic Nd fraction in very good agreement with other archives such as foraminifera (Blaser et al., 2019; Pöppelmeier et al., 2019, 2020), fish debris (Pöppelmeier et al., 2018), and biogenic opal (Huang et al., 2020). Nd was separated from the sample matrix by a two-step column chromatography with 50W-X8 and Ln-Spec resins. The Nd isotopic ratios were measured on a Neptune Plus MC-ICP-MS at GEOMAR Kiel. Instrumental fractionation on isotopic ratios was corrected for by normalizing $^{146}Nd/^{144}Nd$ to 0.7219 with an exponential law. Samples were further bracketed by concentration matched solutions of JNdi-1 reference material normalized to the accepted value of $^{143}Nd/^{144}Nd = 0.512115$ (Tanaka et al., 2000). The external reproducibility for each session was determined by repeated measurements of in-house standards yielding a double standard deviation of 0.1

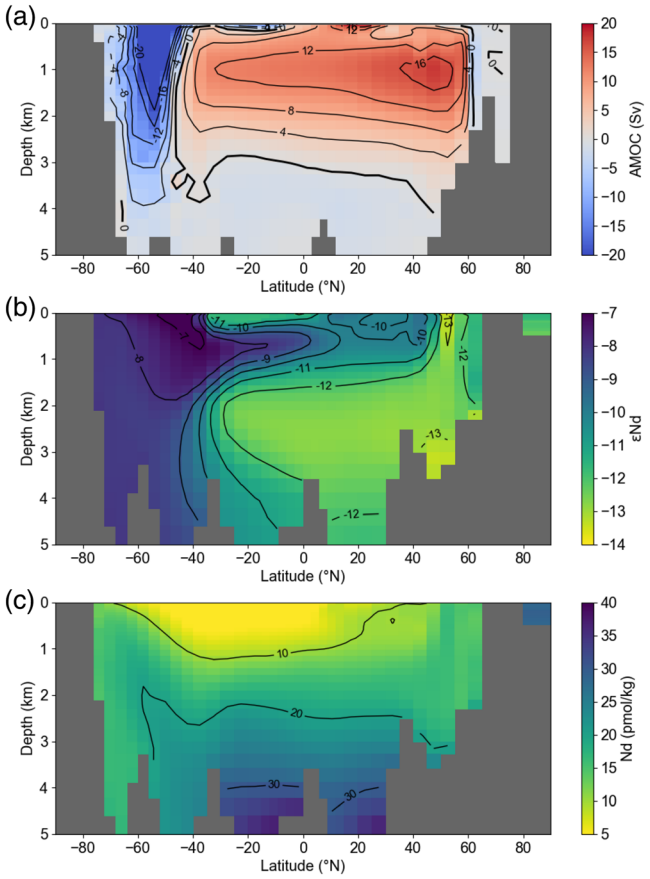

Figure 4. Bern3D control run. (a) Zonally integrated stream function of the Atlantic. (b, c) Nd isotope signatures and dissolved Nd concentrations of the control run along the meridional section at 31.5°W. See section 3.1 for tuned parameters.

to 0.5 ε-units. Total procedural blanks were below 0.1% of the sample sizes and are hence negligible. Mean deviation between total procedure replicates is <0.2 ε-units (Table S5).

3. Results

3.1. Bern3D Control Simulation and Sensitivity Tests

The steady-state AMOC strength simulated in the Bern3D model under preindustrial boundary conditions is 17.7 Sv (Sv: Sverdrup = 10^6 m^3/s), which agrees well with modern observations (e.g., Frajka-Williams et al., 2019), however, with NADW slightly shallower in the model than observed in the modern ocean (Figure 4). As reported by previous studies (Gu et al., 2019; Rempfer et al., 2011), the MAEs of the Nd concentration and ε_{Nd} cannot be minimized with the same set of parameters (Figure S4). Therefore, we choose the following parameters in between the two minima as a compromise: a benthic Nd flux of 3.3×10^9 g/a corresponding to 5.4 pmol/(cm^2 a), a scavenging efficiency parameterized by the ratio of particulate to dissolved Nd concentration of 0.0014 (see Rempfer et al., 2011), and a riverine Nd scaling of 3.5 (corresponding to an increase of all riverine Nd fluxes by a factor of 3.5), yielding a mean Nd residence time of 690 years. With this newly tuned control run, the contributions of the three Nd sources to the total Nd input changed substantially from the implementation by Rempfer et al. (2011). The benthic Nd flux now contributes about 60% to the total Nd input instead of ~90% previously. The riverine and dust fluxes now contribute 32% and 9%, respectively, compared to around 6% and 4% in Rempfer et al. (2011) (see Table S2 for a detailed comparison). The corresponding minimum MAEs for the Nd concentration and ε_{Nd} are 5.3 pmol/kg (n = 1,137) and 1.22 ε-units (n = 1,311), respectively (Figures S8 and S9).

In order to investigate the influence of varying Nd fluxes, potentially caused by changes in the weathering regimes of the northern high latitudes during the last deglaciation (Howe et al., 2016; Pöppelmeier et al., 2019), we performed sensitivity tests by multiplying the benthic Nd flux scaling in the northern North Atlantic in regions with base scaling factors $\alpha_{bs} > 1$ (orange and black areas north of the equator in Figure 3d) by factors of 2, 3, 4, and 5 (Figure 5). This corresponds to Nd fluxes of 0.36, 0.72, 1.08, and 1.44×10^9 g/a in addition to the total Nd flux of 5.55×10^9 g/a in the control run. A doubling of the benthic Nd flux scaling has limited influence on the deep ocean ε_{Nd} distribution only producing slightly less radiogenic (lower) values ($-0.5 < \Delta\varepsilon_{Nd} < 0$) throughout the Atlantic. Tripling of the benthic Nd flux scaling produces a shift of slightly more than 0.5 ε-units less radiogenic signatures in the bulk of NADW and changes smaller than that elsewhere. Quadrupling the benthic Nd flux scaling decreases ε_{Nd} in the core of NADW by more than 1 ε-unit, 0.5 to 1 ε-units in the rest of NADW dominated waters, and less than −0.5 ε-units elsewhere. Finally, multiplying the benthic Nd flux scaling by a factor of 5 produces a shift of more than −1 ε-unit in the bulk of NADW and changes smaller than −0.5 ε-units in southern sourced waters.

3.2. Holocene ε_{Nd} Compilation

In total we compiled 28 Holocene ε_{Nd} records that are located between 45°N and 45°S in the Atlantic and for which no in situ alterations were reported (Table S1). The early Holocene ε_{Nd} anomalies vary between 0 and 1.19 ε-units with an average of 0.72 ± 0.36 (1σ) ε-units (circles in Figure 5). A slight meridional gradient is apparent with highest values in the North Atlantic at around 3,000 m water depth. Sites shallower than 2,000 m generally exhibit smaller to nonexistent early Holocene ε_{Nd} anomalies.

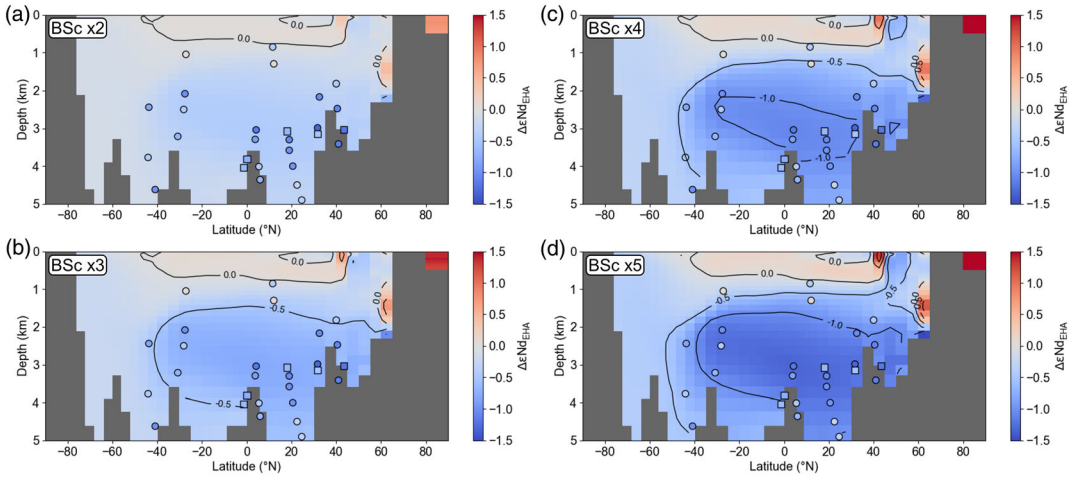

Figure 5. Differences in ε_{Nd} between sensitivity tests and control run along the meridional section at 31.5°W in the Atlantic basin. For the sensitivity simulations the benthic Nd flux scaling (BSc) in the northern North Atlantic (see Figure 3d for details) was multiplied by factors of (a) 2, (b) 3, (c) 4, and (d) 5. Published and new early Holocene anomalies (as defined in section 2.2; Table S1) of the Atlantic between 45°S and 45°N are indicated as circles and squares, respectively, using the same color scale as the model output.

4. Discussion

4.1. Neodymium in the Bern3D Model

The different observational databases used by previous Nd isotope model studies limit the comparability of model performances. However, the implementation of Nd by Rempfer et al. (2011) and Gu et al. (2019) is extremely similar to the one presented here. Both studies also reported MAEs, facilitating a cautious comparison of model performances. The adjustments to the Nd-module of the Bern3D model (as described in section 2.1) improved the model-data agreement for the Nd concentration compared to Rempfer et al. (2011) as well as to Gu et al. (2019), who reported MAEs for their control runs of 9 and 8.1 pmol/kg, respectively. Part of the smaller mismatch found here (5.3 pmol/kg) can be attributed to the exclusion of seawater data from the uppermost 250 m in our approach. Even when considering all water depths including near-surface water, the misfits remain smaller than listed by Rempfer et al. (2011) and Gu et al. (2019) (6.5 pmol/kg; Table S3). Both previous studies reported particularly large deviations in the top 2,000 m of the water column, due to too low Nd concentrations at these depths in the models compared to modern seawater. In the new implementation in the Bern3D model, we do not observe this effect to the same extent in the depth range between 250 and 2,000 m with a MAEs of 5.7 pmol/kg ($n = 711$). The larger surface Nd fluxes associated with the newly introduced scaling factor for the riverine Nd input lead to higher upper ocean Nd concentrations than found in the previous model studies, thus being in better agreement with the observed Nd distribution of the modern ocean (van de Flierdt et al., 2016). This supports the findings by Rousseau et al. (2015) that estuarine dissolution of riverine material plays an important role in the Nd cycle.

Uncertainty estimates are not yet available for measured seawater Nd concentrations accounting for seasonal to decadal variability, as they have been observed on regional scale (Grasse et al., 2017; Yu et al., 2017). However, an intercalibration study for the GEOTRACES program yielded an interlaboratory reproducibility in the order of ±10% (2 standard deviations) for dissolved Nd concentrations (van de Flierdt et al., 2012). Assuming a similar range for the seasonal to decadal variability (Yu et al., 2017) and a global mean Nd concentration of around 20 pmol/kg (Tachikawa et al., 2017) results in a total observational uncertainty in the same range as the model data misfit reported here. This increases the confidence in the new Nd implementation to reasonably represent the Nd cycle of the modern ocean.

The MAE of ε_{Nd} of 1.22 is also improved compared to the studies by Rempfer et al. (2011) and Gu et al. (2019), who reported MAEs of 1.66 and 1.76 ε-units, respectively. However, taking all water depths into account, instead of ignoring the top 250 m, yields a MAE of 1.54 ε-units, which is only slightly lower than found by these two studies (Table S3). This is not surprising, considering that seawater data are strongly biased

toward shallower stations (Tachikawa et al., 2017) and that the surface ocean ε_{Nd} boundary conditions in all three studies are very similar and most susceptible to unknown or minor sources and sinks (see section 2.1). Another important factor that stands in the way of a substantial improvement of the ε_{Nd} misfit is the intermediate complexity of the Bern3D model. For instance, in the Bern3D model deep water formation in the North Atlantic does not produce lower and upper NADW independently as observed in the modern ocean, but instead, only one well-mixed water mass enters the North Atlantic. As such, the well-defined ε_{Nd} characteristics of Labrador Sea Water and the Nordic Seas overflow waters (van de Flierdt et al., 2016) can inherently not be reproduced here, strongly contributing to the calculated model data misfit due to the geographical bias of the observational data toward the Atlantic. Similarly, the different deep ocean circulation patterns of the eastern and western Atlantic basins are not fully resolved in the Bern3D model and also contribute to the misfit. Nevertheless, the overall quasi-conservative behavior of ε_{Nd} is well represented in the model as indicated by the good agreement with the salinity distribution (Figure S5). The implementation presented here thus underscores that the two major controls via a global benthic flux in tandem with dissolution of resuspended riverine material provide a better representation of the global distribution of the Nd concentration than previous parametrizations, without hampering the model's capability to represent the Nd isotopic composition in good agreement with observational data.

4.2. Early Holocene ε_{Nd} Anomaly

A universal benthic flux, as implemented here, could impact the reliability of archived Nd isotope signatures by influencing the authigenic mineral phases through pore-water exchange. Generally, it is assumed that authigenic phases are formed from the pore water at the sediment-water interface. A benthic flux with a different Nd isotope signature than the bottom water could therefore shift the authigenic Nd isotope signature away from the bottom water signature. The extent of such an overprinting not only depends on the strength of the benthic flux itself but also the bottom water advection rate and the differences in ε_{Nd} between bottom water, authigenic phase, and benthic flux (i.e., the local detrital material) (Abbott et al., 2015; Blaser et al., 2020). As such, the implications on down-core ε_{Nd} records may be limited to regions or time periods with strong benthic fluxes isotopically distinct from local bottom water (such as the Labrador Sea and around Iceland) and/or sluggish circulation. Furthermore, both circulation strength and sediment provenance are considered rather invariant during the Holocene in the low-latitude to midlatitude Atlantic, and hence, potential overprinting of reconstructed Nd isotopes of the data presented here can be assumed to be constant. Thus, we can neglect the potential effect of benthic fluxes on archived authigenic phases for the Holocene ε_{Nd} compilation.

The direction toward less radiogenic values of the early Holocene ε_{Nd} anomaly observed ubiquitously in the Atlantic (Howe et al., 2017; Lippold et al., 2016; Roberts et al., 2010) excludes virtually all regions as a source, except the northern Northwest Atlantic, which is surrounded by very old cratons with exceptionally unradiogenic Nd isotopic signatures (as low as < -30; Jeandel et al., 2007). The proposed reason for the negative ε_{Nd} end member shift of -1.4 ± 0.4 ε-units (Pöppelmeier et al., 2019) during the early Holocene is an increased flux of reactive material from North America and Greenland, after the ice sheets retreated subsequently exposing material that was physically weathered by the ice but only poorly chemically weathered (Howe et al., 2016). To test the influence of such elevated Nd fluxes on the Nd isotopic distribution in the Atlantic, we increased the benthic Nd flux scaling throughout the northern North Atlantic with $\alpha_{bs} > 1$ by factors of 2, 3, 4, and 5 (Figure 3d). This elevated Nd flux did arguably not only originate from a benthic source, but rivers draining the glacial lakes that were left behind by the retreating ice sheets likely also contributed to an increased Nd flux (in dissolved form) into the surrounding oceans. However, we argue here that the sedimentary load transported by these rivers and subsequently deposited at the ocean margins was the main source of the elevated Nd flux, since the exchange time with water is orders of magnitudes longer after deposition in the oceans than during riverine transport. Further, we regard incongruent release of less radiogenic Nd during the early Holocene only of subordinate role, because (i) incongruent weathering of Nd is generally found to produce relatively small isotopic differences (Bayon et al., 2015) and (ii) the previous physical weathering by the ice sheet should have increased the fraction of resistant minerals being susceptible to chemical weathering reducing the incongruent release of Nd (Dausmann et al., 2019). Thus, we simplified the parametrization of the elevated Nd flux by only scaling the regional benthic flux in accordance with the intermediate complexity of the Bern3D model. As a consequence, this benthic flux scaling will be an

upper limit and might have been smaller depending on the amount of less radiogenic Nd delivered to the ocean due to incongruent weathering.

The best fit of the sensitivity tests with our compiled observational data of the early Holocene ε_{Nd} anomaly is achieved when multiplying the benthic scaling factor by factors of 3 to 4, producing MAEs of 0.29 and 0.28 ε-units (Figure S11), respectively, which is in the same order as the analytical uncertainty of Nd isotope reconstructions. In contrast, doubling of the scaling factor produces a too small ε_{Nd} deviation from the modern ocean control run, which is reflected in the relatively large MAE of 0.43 ε-units. Further, scaling factors greater than 4 produce too large deviations, indicated by the MAE of 0.40 ε-units for a fivefold benthic flux scaling in the North Atlantic.

The increase in the total global annual Nd flux for the best model data fits is substantial, with close to 13% and 20% for scaling factors of 3 and 4, respectively. This corresponds to local benthic Nd fluxes of up to 65 pmol/(cm^2 a) for the most extreme case. A study from the Oregon margin reported a benthic flux of up to 30 pmol/(cm^2 a) on local scale in the modern Pacific (Abbott et al., 2015). The Oregon margin is influenced by poorly weathered young volcanic and riverine material and thus represents similar sedimentary conditions regarding its reactivity as presumed here for the northern Northwest Atlantic during the late deglaciation/early Holocene. Hence, this similar benthic flux strength indicates that the upper benthic flux limit for such a scenario is reasonable.

In order to test the possibility of an ocean dynamical origin as alternative cause for the Nd isotope variations during the early Holocene, we performed two tests of AMOC strength variations. Simulations were carried out with an ~15% reduced (15.1 Sv) and ~15% strengthened (20.3 Sv) AMOC compared to the control run, while all Nd sources and sinks remained unchanged. A 15% AMOC reduction is the upper limit that could have occurred for more than a few hundred years during the early Holocene, as constrained by high-resolution $^{231}Pa/^{230}Th$ data from the deep Northwest Atlantic (Lippold et al., 2019). The large-scale patterns of the difference between the control run and the scenarios with varied AMOC strength show rather little change in the North Atlantic (generally less than 0.5 ε-units) and a dipole structure in the South Atlantic. For the reduction scenario less radiogenic values at shallow depths are associated with reduced formation of AAIW as a response to reduced NADW formation, which are tightly coupled (e.g., Oppo et al., 2018), and more radiogenic signatures at depth are related to increased proportions of AABW (vice versa for the AMOC increase) (Figure 6). Further, the northern North Atlantic exhibits more radiogenic signatures under a strengthened AMOC due to greater entrainment of AAIW and faster export of unradiogenic Nd with NADW. These ε_{Nd} changes in response to AMOC variations partly contrast the prevailing notion that more radiogenic ε_{Nd} in the North Atlantic is a consequence of increased proportions of AABW. The here presented simulations with varied AMOC strengths thus highlight the complex interactions between various water masses and caution the use of binary mixing assumptions that may have spatially limited validity (i.e., here only valid in the low to midlatitudes below 3,000 m water depth).

To conclude, variations in AMOC strength are unable to explain the homogeneous ε_{Nd} excursions observed during the early Holocene in the Bern3D model. This is also indicated by the rather poor MAEs of compiled early Holocene anomaly data of 0.66 and 0.91 ε-units for the reduction and strengthening scenarios, respectively, when compared to 0.28 ε-units for the scenario featuring a benthic scaling factor of 4. We therefore consider an elevated benthic Nd flux into the northern Northwest Atlantic, caused by exposing chemically poorly weathered material below retreating ice sheets, as the most likely cause for the early Holocene ε_{Nd} anomaly. We note, however, that the deep circulation of the Bern3D model is not capable of resolving the modern hydrography in full detail and hence contributions from changes in the overturning circulation cannot be fully excluded.

4.3. Implications for the Stability of ε_{Nd} End Members

From our modeling results we infer that the North Atlantic ε_{Nd} end member might be strongly influenced by the climatic boundary conditions that determine the continental weathering regime and hence the Nd flux into the oceans. This has profound consequences on the stability of the water mass end member characteristics and thus also on the interpretations of down-core Nd isotope records. An important control determining the contributions from the different continents to the North Atlantic seems to be the extent of the continental ice sheets. Large North American ice sheets, as observed during the LGM, should have

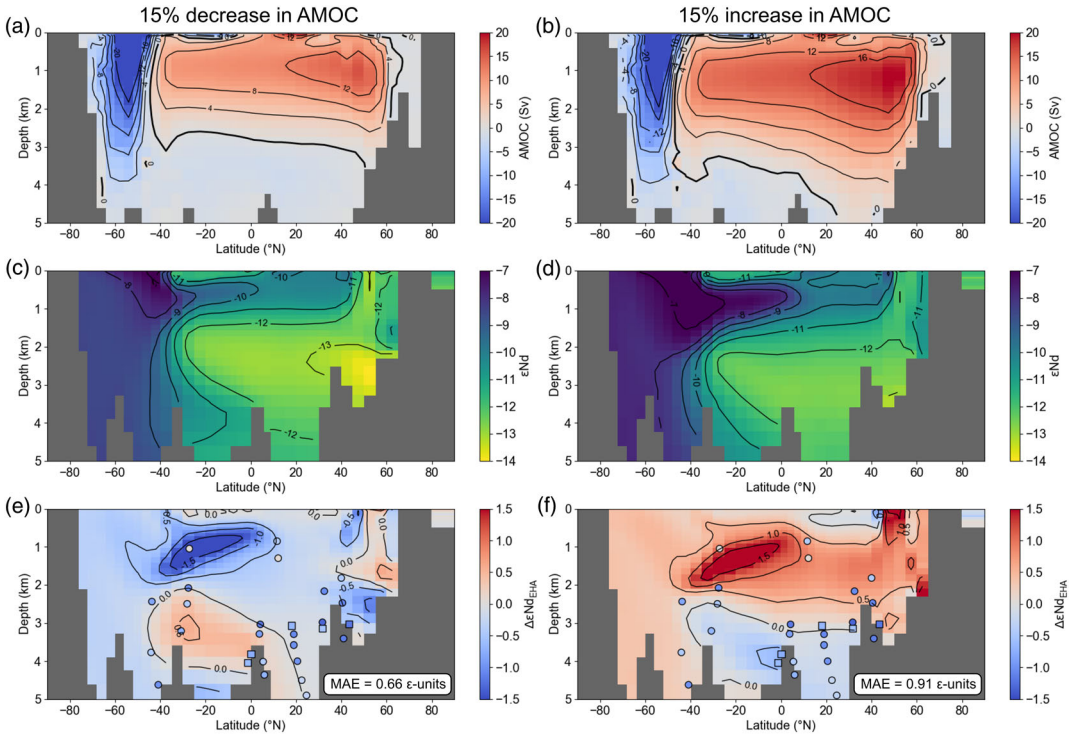

Figure 6. Influence of different AMOC strengths on the Atlantic Nd isotope distribution. (a, b) Stream function of the AMOC varied from 17.7 Sv (Figure 4a) in the control run to 15.1 Sv (a) and 20.3 Sv (b) here (15% reduction/increase). (c, d) ε_{Nd} distributions corresponding to the varied AMOC strengths. (e, f) Difference in ε_{Nd} between panels c/d and the control run. Filled circles and squares mark published and new early Holocene ε_{Nd} anomalies, respectively, on the same scale. MAEs are 0.66 and 0.91 ε-units for a 15% reduction and strengthening, respectively.

limited the supply of unradiogenic material to the northern North Atlantic (Blaser et al., 2020). This would raise the ε_{Nd} end member signature toward more radiogenic signatures, which is confirmed by a recent study reporting such a more radiogenic end member during the LGM (Zhao et al., 2019). During the deglaciation, the retreating North American ice sheets exposed large amounts of poorly chemically weathered unradiogenic material, which accordingly led to an unradiogenic shift of the North Atlantic ε_{Nd} end member signature, as discussed in the present study. During full interglacial times, material originally eroded during the glacial is very efficiently chemically weathered at first (e.g., Middelburg et al., 1988) but successively releases less and less Nd, which explains the gradual change in the Atlantic ε_{Nd} records of the Holocene (Figure 3; Howe et al., 2017; Lippold et al., 2019; Pöppelmeier et al., 2019).

However, migrations of the deep water formation zones and varying contributions of the different water masses to the main water bodies entering the Atlantic can also substantially influence the end member ε_{Nd} signatures. For instance, absence of relatively unradiogenic AABW formation in the Weddell Sea is suggested as the reason for the more radiogenic end member values of southern sourced water during the LGM (Huang et al., 2020). Since the Antarctic ice sheet exposes only little continental areas even during full interglacial times, changes in the weathering regime generally play a smaller role in the Southern Ocean.

The combination of the potential drivers for changes in the ε_{Nd} end member signatures highlights that end members cannot be assumed constant on millennial to glacial-interglacial timescales. Particularly, early interglacial periods may have been prone to substantial northern end member shifts toward less radiogenic signatures analogous to the here investigated early Holocene. A previous study investigating the northern end member over the past 0.5 Ma reported a relatively stable Nd isotope signature based on ferromanganese crusts (Foster et al., 2007). Yet the low accumulation rates of these crusts in the order of mm/Ma make it virtually impossible to resolve such variations considering that a single data point represents an integrated signal over tens of thousands of years. Thus, robust end member constraints are crucial for faithful reconstructions of interbasin water mass mixing with Nd isotopes.

5. Conclusions

We presented new Holocene Nd isotope data complementing published records for an Atlantic-wide compilation of the early Holocene ε_{Nd} anomaly (i.e., the deviation of early Holocene deep Atlantic ε_{Nd} relative to modern compositions). The spatial distribution emergent from this compilation allowed us to assess the potential mechanisms responsible for this feature. In order to test different scenarios and pinpoint the most likely control, we employed the Nd-enabled Bern3D model. For this we updated its Nd-module by including new findings regarding sources and sinks of Nd as well as adjusting the parameterization of the benthic Nd source to extend to all water depths, as indicated by recent investigations. In addition, we implemented a new parameter for the release of Nd from resuspended riverine material. The new Nd implementation substantially reduced the model data misfit of the dissolved Nd concentration as well as ε_{Nd} compared to previous studies. In the control run Nd has a global mean residence time of 690 years in agreement with previous estimates. The contributions to the total Nd source are now divided into ~60% boundary/benthic source, ~32% riverine source, and ~9% dust.

We tested the hypothesis of an elevated Nd flux into the northern North Atlantic due to an increased supply of poorly chemically weathered material as a cause for the early Holocene ε_{Nd} anomaly by scaling the benthic Nd flux in the respective regions by different factors. We achieved a best model data fit by an increase in the benthic flux by a factor between 3 and 4, which also reproduces the spatial distribution of the early Holocene ε_{Nd} anomaly of the data compilation in good agreement. This scaling factor represents an upper limit, because changes in the isotopic composition of the supplied material (e.g., due to incongruent weathering) are not considered here.

We thus conclude that the early Holocene ε_{Nd} anomalies observed throughout the deep Atlantic are best explained by an increased input of Nd into the northern high latitudes during the time of final continental ice sheet retreat. Even though the amount of Nd required to reproduce the ε_{Nd} excursions is substantial, the impact beyond the NADW dominated region is small, in agreement with observations. As such, this contrasts the pattern of Nd isotope changes caused by variations in the AMOC strength during the early Holocene, which are less homogeneous and also affect regions outside the limit of NADW. The model simulations show that northern ε_{Nd} end member changes can be clearly distinguished from changes associated with AMOC reorganizations by their respective large-scale patterns. This places caution on interpretations of single ε_{Nd} records but highlights the strength of compilations extending beyond the domain of one water mass.

Data Availability Statement

Data of this study can be found in the supporting information and on Pangaea (https://doi.pangaea.de/10.1594/PANGAEA.922992).

Acknowledgments

Sediment material was provided by the ODP/IODP core repository Bremen and the GeoTü repository of the University of Tübingen. We thank Hartmut Schulz for help with sampling and sedimentary analyses. Norbert Frank and Sönke Szidat are thanked for analytical support. Simulations were performed on UBELIX, the HPC cluster at the University of Bern. This is TiPES Contribution 44. F. P. and T. F. S. acknowledge financial support from the European Union's Horizon 2020 research and innovation program under Grant Agreement No. 820970. J. L. and P. B. are supported by the Emmy-Noether Programme of the German Research Foundation (Grant Li1815/4). T. F. S. and J. S. acknowledge financial support from the Swiss National Science Foundation (SNSF Grant 200020-172745). We thank three anonymous reviewers for thoughtful comments that helped to improve the manuscript.

References

Abbott, A. N. (2019). A benthic flux from calcareous sediments results in non-conservative neodymium behavior during lateral transport: A study from the Tasman Sea. *Geology*, *47*(4), 363–366. https://doi.org/10.1130/G45904.1

Abbott, A. N., Haley, B. A., & McManus, J. (2015). Bottoms up: Sedimentary control of the deep North Pacific Ocean's ε_{Nd} signature. *Geology*, *43*(11), 1035–1038. https://doi.org/10.1130/G37114.1

Amakawa, H., Yu, T. L., Tazoe, H., Obata, H., Gamo, T., Sano, Y., et al. (2019). Neodymium concentration and isotopic composition distributions in the southwestern Indian Ocean and the Indian sector of the Southern Ocean. *Chemical Geology*, *511*, 190–203. https://doi.org/10.1016/j.chemgeo.2019.01.007

Andersen, K. K., Azuma, N., Barnola, J. M., Bigler, M., Biscaye, P., Caillon, N., et al. (2004). High-resolution record of Northern Hemisphere climate extending into the last interglacial period. *Nature*, *431*(7005), 147–151. https://doi.org/10.1038/nature02805

Arsouze, T., Dutay, J. C., Lacan, F., & Jeandel, C. (2007). Modeling the neodymium isotopic composition with a global ocean circulation model. *Chemical Geology*, *239*(1–2), 165–177. https://doi.org/10.1016/j.chemgeo.2006.12.006

Arsouze, T., Dutay, J.-C., Lacan, F., & Jeandel, C. (2009). Reconstructing the Nd oceanic cycle using a coupled dynamical-biogeochemical model. *Biogeosciences*, *6*(3), 5549–5588. https://doi.org/10.5194/bgd-6-5549-2009

Bayon, G., Toucanne, S., Skonieczny, C., André, L., Bermell, S., Cheron, S., et al. (2015). Rare earth elements and neodymium isotopes in world river sediments revisited. *Geochimica et Cosmochimica Acta*, *170*, 17–38. https://doi.org/10.1016/j.gca.2015.08.001

Blanchet, C. L. (2019). A database of marine and terrestrial radiogenic Nd and Sr isotopes for tracing earth-surface processes. *Earth System Science Data*, *11*(2), 741–759. https://doi.org/10.5194/essd-11-741-2019

Blaser, P., Gutjahr, M., Pöppelmeier, F., Frank, M., Kaboth-Bahr, S., & Lippold, J. (2020). Labrador Sea bottom water provenance and REE exchange over the past 35,000 years. *Earth and Planetary Science Letters*, *542*, 116299. https://doi.org/10.1016/j.epsl.2020.116299

Blaser, P., Lippold, J., Gutjahr, M., Frank, N., Link, J. M., & Frank, M. (2016). Extracting foraminiferal seawater Nd isotope signatures from bulk deep sea sediment by chemical leaching. *Chemical Geology*, *439*, 189–204. https://doi.org/10.1016/j.chemgeo.2016.06.024

Blaser, P., Pöppelmeier, F., Schulz, H., Gutjahr, M., Frank, M., Lippold, J., et al. (2019). The resilience and sensitivity of Northeast Atlantic deep water εNd to overprinting by detrital fluxes over the past 30,000 years. *Geochimica et Cosmochimica Acta*, *245*, 79–97. https://doi.org/10.1016/j.gca.2018.10.018

Casse, M., Montero-Serrano, J.-C., St-Onge, G., & Poirier, A. (2019). REE distribution and Nd isotope composition of estuarine waters and bulk sediment leachates tracing lithogenic inputs in eastern Canada. *Marine Chemistry*, *211*, 117–130. https://doi.org/10.1016/j.marchem.2019.03.012

Dai, A., & Trenberth, K. E. (2002). Estimates of freshwater discharge from continents: Latitudinal and seasonal variations. *Journal of Hydrometeorology*, *3*, 660–687. https://doi.org/10.1175/1525-7541(2002)003<0660:EOFDFC>2.0.CO;2

Dausmann, V., Gutjahr, M., Frank, M., Kouzmanov, K., & Schaltegger, U. (2019). Experimental evidence for mineral-controlled release of radiogenic Nd, Hf and Pb isotopes from granitic rocks during progressive chemical weathering. *Chemical Geology*, *507*, 64–84. https://doi.org/10.1016/j.chemgeo.2018.12.024

Elmore, A. C., Piotrowski, A. M., Wright, J. D., & Scrivner, A. E. (2011). Testing the extraction of past seawater Nd isotopic composition from North Atlantic deep sea sediments and foraminifera. *Geochemistry, Geophysics, Geosystems*, *12*, Q09008. https://doi.org/10.1029/2011GC003741

Foster, G. L., Vance, D., & Prytulak, J. (2007). No change in the neodymium isotope composition of deep water exported from the North Atlantic on glacial-interglacial time scales. *Geology*, *35*(1), 37–40. https://doi.org/10.1130/G23204A.1

Frajka-Williams, E., Ansorge, I. J., Baehr, J., Bryden, H. L., Chidichimo, M. P., Cunningham, S. A., et al. (2019). Atlantic meridional overturning circulation: Observed transport and variability. *Frontiers in Marine Science*, *6*, 1–18. https://doi.org/10.3389/fmars.2019.00260

Friedrich, T., Timmermann, A., Stichel, T., & Pahnke, K. (2014). Ocean circulation reconstructions from ε_{Nd}: A model-based feasibility study. *Paleoceanography*, *29*, 1–21. https://doi.org/10.1002/2014PA002658

Goldstein, S. J., & Jacobsen, S. B. (1987). The Nd and Sr isotopic systematics of river-water dissolved material implications for the sources of Nd and Sr in seawater. *Chemical Geology*, *66*, 245–272. https://doi.org/10.1016/0168-9622(87)90045-5

Goldstein, S. J., & Jacobsen, S. B. (1988). Rare earth elements in river waters. *Earth and Planetary Science Letters*, *89*(1), 35–47. https://doi.org/10.1016/0012-821X(88)90031-3

Grasse, P., Bosse, L., Hathorne, E. C., Böning, P., Pahnke, K., & Frank, M. (2017). Short-term variability of dissolved rare earth elements and neodymium isotopes in the entire water column of the Panama Basin. *Earth and Planetary Science Letters*, *475*, 242–253. https://doi.org/10.1016/j.epsl.2017.07.022

Grenier, M., Jeandel, C., Lacan, F., Vance, D., Venchiarutti, C., Cros, A., & Cravatte, S. (2013). From the subtropics to the central equatorial Pacific Ocean: Neodymium isotopic composition and rare earth element concentration variations. *Journal of Geophysical Research: Oceans*, *118*, 592–618. https://doi.org/10.1029/2012JC008239

Gu, S., Liu, Z., Jahn, A., Rempfer, J., Zhang, J., & Joos, F. (2019). Modeling neodymium isotopes in the ocean component of the Community Earth System Model (CESM1). *Journal of Advances in Modeling Earth Systems*, *11*, 624–640. https://doi.org/10.1029/2018MS001538

Haley, B. A., Du, J., Abbott, A. N., & McManus, J. (2017). The impact of benthic processes on rare earth element and neodymium isotope distributions in the oceans. *Frontiers in Marine Science*, *4*, 1–12. https://doi.org/10.3389/fmars.2017.00426

Howe, J. N. W., Piotrowski, A. M., Hu, R., & Bory, A. (2017). Reconstruction of east-west deep water exchange in the low latitude Atlantic Ocean over the past 25,000 years. *Earth and Planetary Science Letters*, *458*, 327–336. https://doi.org/10.1016/j.epsl.2016.10.048

Howe, J. N. W., Piotrowski, A. M., & Rennie, V. C. F. (2016). Abyssal origin for the early Holocene pulse of unradiogenic neodymium isotopes in Atlantic seawater. *Geology*, *44*(10), 831–834. https://doi.org/10.1130/G38155.1

Huang, H., Gutjahr, M., Eisenhauer, A., & Kuhn, G. (2020). No detectable Weddell Sea Antarctic bottom water export during the last and penultimate glacial maximum. *Nature Communications*, *11*(1), 1–10. https://doi.org/10.1038/s41467-020-14302-3

Jacobsen, S. B., & Wasserburg, G. J. (1980). Sm-Nd isotopic evolution of chondrites. *Earth and Planetary Science Letters*, *50*(1), 139–155. https://doi.org/10.1016/0012-821X(80)90125-9

Jeandel, C., Arsouze, T., Lacan, F., Téchiné, P., & Dutay, J. C. (2007). Isotopic Nd compositions and concentrations of the lithogenic inputs into the ocean: A compilation, with an emphasis on the margins. *Chemical Geology*, *239*(1–2), 156–164. https://doi.org/10.1016/j.chemgeo.2006.11.013

Lacan, F., & Jeandel, C. (2005). Acquisition of the neodymium isotopic composition of the North Atlantic Deep Water. *Geochemistry, Geophysics, Geosystems*, *6*, Q12008. https://doi.org/10.1029/2005GC000956

Lambelet, M., van de Flierdt, T., Crocket, K., Rehkämper, M., Kreissig, K., Coles, B., et al. (2016). Neodymium isotopic composition and concentration in the western North Atlantic Ocean: Results from the GEOTRACES GA02 section. *Geochimica et Cosmochimica Acta*, *177*, 1–29. https://doi.org/10.1016/j.gca.2015.12.019

Lippold, J., Gutjahr, M., Blaser, P., Christner, E., de Carvalho Ferreira, M. L., Mulitza, S., et al. (2016). Deep water provenance and dynamics of the (de)glacial Atlantic meridional overturning circulation. *Earth and Planetary Science Letters*, *445*, 68–78. https://doi.org/10.1016/j.epsl.2016.04.013

Lippold, J., Pöppelmeier, F., Süfke, F., Gutjahr, M., Goepfert, T. J., Blaser, P., et al. (2019). Constraining the variability of the Atlantic Meridional Overturning Circulation during the Holocene. *Geophysical Research Letters*, *46*, 11,338–11,346. https://doi.org/10.1029/2019GL084988

Mahowald, N. M., Muhs, D. R., Levis, S., Rasch, P. J., Yoshioka, M., Zender, C. S., & Luo, C. (2006). Change in atmospheric mineral aerosols in response to climate: Last glacial period, preindustrial, modern, and doubled carbon dioxide climates. *Journal of Geophysical Research*, *111*, D10202. https://doi.org/10.1029/2005JD006653

Middelburg, J. J., van der Weijden, C. H., & Woittiez, J. R. W. (1988). Chemical processes affecting the mobility of major, minor and trace elements during weathering of granitic rocks. *Chemical Geology*, *68*(3–4), 253–273. https://doi.org/10.1016/0009-2541(88)90025-3

Müller, S. A., Joos, F., Edwards, N. R., & Stocker, T. F. (2006). Water mass distribution and ventilation time scales in a cost-efficient, three dimensional ocean model. *Journal of Climate*, *19*(21), 5479–5499. https://doi.org/10.1175/JCLI3911.1

Oppo, D. W., Gebbie, G., Huang, K. F., Curry, W. B., Marchitto, T. M., & Pietro, K. R. (2018). Data constraints on glacial Atlantic water mass geometry and properties. *Paleoceanography and Paleoclimatology*, *33*, 1013–1034. https://doi.org/10.1029/2018PA003408

Piotrowski, A. M., Goldstein, S. L., Hemming, S. R., & Fairbanks, R. G. (2005). Temporal relationships of carbon cycling and ocean circulation at glacial boundaries. *Science*, *307*(5717), 1933–1938. https://doi.org/10.1126/science.1104883

Pöppelmeier, F., Blaser, P., Gutjahr, M., Süfke, F., Thornalley, D. J. R., Grützner, J., et al. (2019). Influence of ocean circulation and benthic exchange on deep Northwest Atlantic Nd isotope records during the past 30,000 years. *Geochemistry, Geophysics, Geosystems*, *20*, 4457–4469. https://doi.org/10.1029/2019GC008271

Pöppelmeier, F., Gutjahr, M., Blaser, P., Keigwin, L. D., & Lippold, J. (2018). Origin of abyssal NW Atlantic water masses since the Last Glacial Maximum. *Paleoceanography and Paleoclimatology*, *33*, 530–543. https://doi.org/10.1029/2017PA003290

Pöppelmeier, F., Gutjahr, M., Blaser, P., Oppo, D. W., Jaccard, S. L., Regelous, M., et al. (2020). Water mass gradients of the mid-depth Southwest Atlantic during the past 25,000 years. *Earth and Planetary Science Letters*, *531*, 115963. https://doi.org/10.1016/j.epsl.2019.115963

Rahlf, P., Hathorne, E., Laukert, G., Gutjahr, M., Weldeab, S., & Frank, M. (2020). Tracing water mass mixing and continental inputs in the southeastern Atlantic Ocean with dissolved neodymium isotopes. *Earth and Planetary Science Letters*, *1*, 115944. https://doi.org/10.1016/j.epsl.2019.115944

Rempfer, J., Stocker, T. F., Joos, F., Dutay, J. C., & Siddall, M. (2011). Modelling Nd-isotopes with a coarse resolution ocean circulation model: Sensitivities to model parameters and source/sink distributions. *Geochimica et Cosmochimica Acta*, *75*(20), 5927–5950. https://doi.org/10.1016/j.gca.2011.07.044

Ritz, S. P., Stocker, T. F., & Joos, F. (2011). A coupled dynamical ocean-energy balance atmosphere model for paleoclimate studies. *Journal of Climate*, *24*(2), 349–375. https://doi.org/10.1175/2010JCLI3351.1

Roberts, N. L., & Piotrowski, A. M. (2015). Radiogenic Nd isotope labeling of the northern NE Atlantic during MIS 2. *Earth and Planetary Science Letters*, *423*, 125–133. https://doi.org/10.1016/j.epsl.2015.05.011

Roberts, N. L., Piotrowski, A. M., McManus, J. F., & Keigwin, L. D. (2010). Synchronous deglacial overturning and water mass source changes. *Science*, *327*(5961), 75–78. https://doi.org/10.1126/science.1178068

Rousseau, T. C. C., Sonke, J. E., Chmeleff, J., Van Beek, P., Souhaut, M., Boaventura, G., et al. (2015). Rapid neodymium release to marine waters from lithogenic sediments in the Amazon estuary. *Nature Communications*, *6*(1), 1–8. https://doi.org/10.1038/ncomms8592

Siddall, M., Khatiwala, S., van de Flierdt, T., Jones, K., Goldstein, S. L., Hemming, S., & Anderson, R. F. (2008). Towards explaining the Nd paradox using reversible scavenging in an ocean general circulation model. *Earth and Planetary Science Letters*, *274*(3–4), 448–461. https://doi.org/10.1016/j.epsl.2008.07.044

Stichel, T., Frank, M., Rickli, J., & Haley, B. A. (2012). The hafnium and neodymium isotope composition of seawater in the Atlantic sector of the Southern Ocean. *Earth and Planetary Science Letters*, *317–318*, 282–294. https://doi.org/10.1016/j.epsl.2011.11.025

Stichel, T., Hartman, A. E., Duggan, B., Goldstein, S. L., Scher, H., & Pahnke, K. (2015). Separating biogeochemical cycling of neodymium from water mass mixing in the eastern North Atlantic. *Earth and Planetary Science Letters*, *412*, 245–260. https://doi.org/10.1016/j.epsl.2014.12.008

Stichel, T., Pahnke, K., Duggan, B., Goldstein, S. L., Hartman, A. E., Paffrath, R., & Scher, H. D. (2018). TAG plume: Revisiting the hydrothermal neodymium contribution to seawater. *Frontiers in Marine Science*, *5*(96). https://doi.org/10.3389/fmars.2018.00096

Tachikawa, K., Arsouze, T., Bayon, G., Bory, A., Colin, C., Dutay, J. C., et al. (2017). The large-scale evolution of neodymium isotopic composition in the global modern and Holocene ocean revealed from seawater and archive data. *Chemical Geology*, *457*, 131–148. https://doi.org/10.1016/j.chemgeo.2017.03.018

Tanaka, T., Togashi, S., Kamioka, H., Amakawa, H., Kagami, H., Hamamoto, T., et al. (2000). JNdi-1: A neodymium isotopic reference in consistency with LaJolla neodymium. *Chemical Geology*, *168*(3–4), 279–281. https://doi.org/10.1016/S0009-2541(00)00198-4

van de Flierdt, T., Grifths, A. M., Lambelet, M., Little, S. H., Stichel, T., & Wilson, D. J. (2016). Neodymium in the oceans: A global database, a regional comparison and implications for palaeoceanographic research. *Philosophical Transactions of the Royal Society A: Mathematical, Physical and Engineering Sciences*, *374*(2081). https://doi.org/10.1098/rsta.2015.0293

van de Flierdt, T., Pahnke, K., Amakawa, H., Andersson, P., Basak, C., Coles, B., et al. (2012). GEOTRACES intercalibration of neodymium isotopes and rare earth element concentrations in seawater and suspended particles. Part 1: Reproducibility of results for the international intercomparison. *Limnology and Oceanography: Methods*, *10*(4), 234–251. https://doi.org/10.4319/lom.2012.10.234

van de Flierdt, T., Robinson, L. F., & Adkins, J. F. (2010). Deep-sea coral aragonite as a recorder for the neodymium isotopic composition of seawater. *Geochimica et Cosmochimica Acta*, *74*(21), 6014–6032. https://doi.org/10.1016/j.gca.2010.08.001

Yu, Z., Colin, C., Meynadier, L., Douville, E., Dapoigny, A., Reverdin, G., et al. (2017). Seasonal variations in dissolved neodymium isotope composition in the Bay of Bengal. *Earth and Planetary Science Letters*, *479*, 310–321. https://doi.org/10.1016/j.epsl.2017.09.022

Zhao, N., Oppo, D. W., Huang, K. F., Howe, J. N. W., Blusztajn, J., & Keigwin, L. D. (2019). Glacial–interglacial Nd isotope variability of North Atlantic Deep Water modulated by North American ice sheet. *Nature Communications*, *10*(1), 1–10. https://doi.org/10.1038/s41467-019-13707-z

Zieringer, M., Frank, M., Stumpf, R., & Hathorne, E. C. (2019). The distribution of neodymium isotopes and concentrations in the eastern tropical North Atlantic. *Chemical Geology*, *511*, 265–278. https://doi.org/10.1016/j.chemgeo.2018.11.024